LETTER

Ordering kinetics in active polar fluid

To cite this article: Shambhavi Dikshit and Shradha Mishra 2023 *EPL* **143** 17001

A Letters Journal Exploring the Frontiers of Physics

July 2023

EPL, **143** (2023) 17001 www.epljournal.org
doi: 10.1209/0295-5075/acdcb6

Ordering kinetics in active polar fluid

Shambhavi Dikshit[(a)] and Shradha Mishra[(b)]

Indian Institute of Technology (BHU) - Varanasi, 221005, India

received 23 January 2023; accepted in final form 8 June 2023
published online 26 June 2023

Abstract – We model the active polar fluid as a collection of orientable objects supplied with active stresses and momentum damping coming from the viscosity of bulk fluid medium. The growth kinetics of local orientation field is studied. The effect of active fluid is contractile or extensile depending upon the sign of the active stress. We explore the growth kinetics for different activities. We observe that for both extensile and contractile cases the growth is altered by a prefactor when compared to the equilibrium *Model A*. We find that the extensile fluid enhances the domain growth whereas the contractile fluid supresses it. The asymptotic growth becomes pure algebraic for large magnitudes of activity. We also find that the domain morphology remains unchanged due to activity and the system shows the good dynamic scaling for all activities. Our study provides the understanding of ordering kinetics in active polar gel.

Introduction. – The systems in which the energy consumption occurs on individual constituent level and leads to collective dynamics are active systems [1,2]. The existence of active systems is found from small microscopic length scale, *i.e.*, interacellular level like cytoskeletal actin filaments [3], bacterial colonies [4], etc. to large macroscopic scale, *i.e.*, up to few meters like animal herds [5], birds flocks [6,7], etc. Active systems are defined as wet when coupled to a momentum conserving solvent, in which solvent-mediated hydrodynamic interaction becomes important [1,2]. Bacterial swarms in a fluid, cytoskeleton filaments, colloidal or nanoscale particles propelled through a fluid are examples of wet systems [8,9]. When no such fluid is present, then the system is called dry. Dry systems include bacteria gliding on a surface [10], animal herds or vibrated granular particles and so on [11,12].

Starting with the seminal work of Vicsek [7], most of the previous works on active system have focused on the steady state properties [1,13–15]. The study of ordering kinetics in active systems is made complex by the fact that the system relaxes to a nonequilibrium steady state (NESS). There have been very few studies [16–19] of the coarsening kinetics from a homogeneous initial state to the asymptotic NESS, though understanding it is of great experimental interest. Previous studies of coarsening or domain growth have primarily focused upon systems approaching to an equilibrium state [20–23]. Based on the symmetry and conservation laws the domain growth is classified mainly in two types. The domain growth in systems with conserved order parameter is named *Model B* and with nonconserved order parameter is called *Model A*, and follows an algebraic growth law with growth exponent $z = 3$ [22] and 2 [23], respectively. For the systems with scalar order parameter and nonconserved growth kinetics, the interfacial velocity of the growing domain is proportional to the local curvature of the interface, which leads to the size of the domain $L(t) \propto t^{1/2}$, Allen and Cahn growth law [24]. On the other hand, for the systems with conserved kinetics the interface has to pay a cost due to local conservation of order parameter. That leads to the size of the domain growing with time such that $L(t) \propto t^{1/3}$ following the Lifshitz-Slyozov-Wagner (LSW) theory [22,25].

For the systems having symmetries of two-dimensional XY-model, with nonconserved growth kinetics and order parameter with more than one components or vector order parameter, the asymptotic growth law is still $z = 2$. The topological defects are vortices and antivortices and the domain growth is driven by the annihilation of these defects. The detailed calculation [26,27] shows that there is logarithmic correction to the pure algebraic growth $L(t) \propto (t/\ln(t))^{1/2}$. Equilibrium liquid crystals, ferromagnetic materials with continuous symmetry, spin glasses, two-dimensional superconductors, etc. are some of the examples of systems with nonconserved vector order parameter.

The domain growth in systems approaching towards a thermal equilibrium state is very well studied in dry [22, 23,26,27] as well as wet systems with hydrodynamic effect [28–31]. The understanding of the ordering kinetics

[(a)]E-mail: shambhavidikshit.rs.phy18@itbhu.ac.in (corresponding author)
[(b)]E-mail: smishra.phy@iitbhu.ac.in

in terms of the number of topological defects is explored in many of the studies [32–36]. Recently some studies are performed on the understanding of ordering of domain growth in *dry* active systems [16,18,19,37]. But the ordering kinetics in active systems *with fluid* is rarely explored. Some recent studies show the effect of hydrodynamics on the ordering kinetics of apolar order parameter field [38] and the effect of fluid on the steady state properties of active polar fluid [39–41]. This motivates us to study the ordering kinetics of active polar systems with fluid or active polar gel. The examples of active polar gels are bacteria suspensions, active emulsions and active gels. [42,43].

The model contains a collection of orientable objects supplied with active stresses and momentum damping coming from the viscosity of bulk fluid medium. The ordering kinetics of the orientational field is studied after a quench from the random disordered state. With time the system orders and the size of ordered domain grows with time. We characterise the domain growth and scaling. The direction of spontaneous flow makes the system respond like extensile and contractile in nature. For the extensile case, particles act like pushers (pulling fluid inward equatorially and emitting it axially) and for contractile case they are more likely pullers [44] (vice versa). We observe that for both extensile and contractile cases the growth is altered by a prefactor when compared to the equilibrium *Model A*. We find that the extensile fluid enhances the domain growth whereas the contractile fluid supresses it. The asymptotic growth becomes pure algebraic for large magnitudes of activity. For all activities, system shows good dynamic scaling and domain morphology remains unaffected with respect to the activity.

Model A. – The time evolution of a system with nonconserved local order parameter for a collection of orientable objects is described by the time-dependent Ginzburg Landau equation [23,45],

$$\frac{\partial P_\alpha(\mathbf{r},t)}{\partial t} = -\Gamma_0 \frac{\delta F_0}{\delta P_\alpha(\mathbf{r},t)} + \theta_\alpha(\mathbf{r},t), \tag{1}$$

where Γ_0 is the mobility. The Ginzburg Landau free energy F_0 is

$$F_0 = \int \mathrm{d}^d r \left\{ \frac{1}{2} a \mathbf{P}(\mathbf{r},t)^2 + \frac{\lambda}{2} |\nabla \mathbf{P}(\mathbf{r},t)^2| + \frac{b}{4} \mathbf{P}(\mathbf{r},t)^4 \right\}, \tag{2}$$

here $\mathbf{P}(\mathbf{r},t)$ is a vector field with components $P_\alpha(r,t)$, and $\alpha = 1$ and 2 in two-dimensions. The vector field $\mathbf{P}(\mathbf{r},t)$ is the local orientation field and is defined by the average orientation of the particles in a small coarse-grained region. The size of the region is such that it consists of sufficient number of particles to perform the statistical averaging. $\theta_\alpha(\mathbf{r},t)$ is Gaussian random white noise with properties $\langle \theta_\alpha(\mathbf{r},t) \rangle = 0$ and $\langle \theta_\alpha(\mathbf{r},t) \theta_\alpha(\mathbf{r}',t') \rangle = 2\Delta_0 \delta(t-t') \delta_{\alpha\alpha'}$. a, b and λ are constants. ($a < 0$ ensures the broken symmetry state, $b > 0$ and $\lambda > 0$ for stability and the strength of noise $\Delta_0 = 0$). After substituting the form of F_0 from eq. (2) in eq. (1) and performing the functional derivative of Ginzburg Landau free energy F_0, we get the time-dependent Ginzburg Landau (TDGL) [23] equation for nonconserved vector field,

$$\frac{\partial \mathbf{P}(\mathbf{r},t)}{\partial t} = a\Gamma_0 \mathbf{P}(\mathbf{r},t) - b\Gamma_0 |\mathbf{P}(\mathbf{r},t)|^2 \mathbf{P}(\mathbf{r},t) + \lambda \nabla^2 \mathbf{P}(\mathbf{r},t). \tag{3}$$

The model described by eq. (3) is called as *Model A* according to Halprin and Hohenberg [23]. The noise term present in eq. (1) is *turned off* and we consider the deterministic part of the TDGL equation as discussed in [21]. The Gaussian noise in eq. (1) is purely thermal in nature and ensures that the system reaches the global minima at late times. But most of the kinetic theories are developed for the deterministic TDGL equation and thermal noise is irrelevant for growth kinetics [21]. Equation (3) very well explains the ordering kinetics in magnets with vector order parameter [46] and liquid crystals [47]. Now we further introduce the effect of hydrodynamic interaction on the ordering kinetics of nonconserved field.

Active polar fluid. – Now we discuss the hydrodnyamics of active polar fluid or active polar gel. We focus here on the active gel defined with a collection of orientable objects supplied with active stresses and momentum damping coming from the viscosity of bulk fluid medium, compared to the friction due to substrate or medium [32,33,41]. The equations are first proposed by [33] for self-propelling objects but later developed by [41] and [32] for the system of cytoskeleton in living cells and polar actin filament, which become active only in the presence of molecular motors that consume ATP. A collection of artificial Janus rods which gain motility due to electrophoresis is a good example of active polar gel and can be easily designed in the laboratory [8]. The presence of fluid introduces the hydrodynamic effect. If the hydrodynamic interaction is turned off then the model is purely passive and the same as *Model A*. The model incorporates the coupling between local order parameter and fluid.

We model the system by the coupled dynamics of the orientation order parameter $\mathbf{P}(\mathbf{r},t)$ with a solvent local velocity $\mathbf{v}(\mathbf{r},t)$ with additional active stresses. The system is modeled by the coarse-grained coupled hydrodynamic non-linear partial differential equations of motion for the two fields. The fluid is introduced through the standard Navier-Stokes equation of motion for fluid with additional coupling to the polarisation, $\mathbf{P}(\mathbf{r},t)$ of particle through active and passive stresses (deviatoric stress) as introduced in [41].

In the presence of fluid, in addition to the term present in eq. (3) coupling to the fluid velocity, eq. (3) will have convective nonlinearity of type $(\mathbf{v}\cdot\nabla)\mathbf{P}$. Hence the modified equation for the $\mathbf{P}(\mathbf{r},t)$ will become

$$\frac{\partial \mathbf{P}(\mathbf{r},t)}{\partial t} + \mathbf{v}\cdot\nabla\mathbf{P}(\mathbf{r},t) + \omega_{\alpha\beta}P_\beta + v_1 v_{\alpha\beta} P_\beta = a\Gamma_0 \mathbf{P}(\mathbf{r},t) - b\Gamma_0 |\mathbf{P}(\mathbf{r},t)|^2 \mathbf{P}(\mathbf{r},t) + \lambda \nabla^2 \mathbf{P}(\mathbf{r},t), \tag{4}$$

with the comoving and corotational derivative of the polarisation, $\mathbf{P}(\mathbf{r},t)$, where $\omega_{\alpha\beta} = \frac{1}{2}(\partial_\alpha v_\beta - \partial_\beta v_\alpha)$ and $v_{\alpha\beta} = \frac{1}{2}(\partial_\alpha v_\beta + \partial_\beta v_\alpha)$ are the vorticity and strain-rate tensor respectively. The coupled velocity field is due to momentum conserving solvent which satisfies the condition of incompressibility, *i.e.*, $\nabla \cdot \mathbf{v} = 0$

The equation for fluid velocity, $\mathbf{v}(\mathbf{r},t)$, satisfying conservation of mass (condition of incompressibility) and conservation of momentum is given as

$$\frac{\partial \mathbf{v}}{\partial t} + \mathbf{v}\cdot\nabla\mathbf{v} = \eta\nabla^2\mathbf{v} - \nabla p + \nabla\cdot\sigma^{total}_{\alpha\beta}. \tag{5}$$

Equation (5) is the Navier-Stokes equation with an additional force term due to stresses present in the fluid.

This term includes the fluid static part and fluid dynamic part that involves activity and flow coupling coefficient. In this case the total stress tensor becomes $\sigma^{total}_{\alpha\beta} = \sigma_{\alpha\beta} + \sigma^{a}_{\alpha\beta}$ where $\sigma_{\alpha\beta}$ is fluid passive part and $\sigma^{a}_{\alpha\beta}$ gives the fluid active part. In polar liquid, mechanical stress tensor can be decomposed into symmetric and antisymmetric part, where the symmetric part of stress tensor is the actual thermodynamics flux and conjugate force is the antisymmetric part of the velocity gradient $v_{\alpha\beta}$. Hence the constitutive equation for stress tensor gives [48]

$$\sigma^{total}_{\alpha\beta} = 2\eta_1 v_{\alpha\beta} + \frac{1}{2}v_1(P_\alpha h_\beta + P_\beta h_\alpha - \frac{d}{2}(P_\gamma h_\gamma \delta_{\alpha\beta})) + \xi q_{\alpha\beta}, \tag{6}$$

here $d = 2$ for the two-dimensions. ξ is the transport coefficient related to the activity of the system. The term $\xi q_{\alpha\beta}$ is self-propelled stress, first incorporated by [49] into generalised hydrodynamics of orientable fluid. The sign of the activity coefficient, ξ tends to change the nature of the system. A negative ξ corresponds to a contractile stress as in the polar active filament [41,48]. A positive ξ shows an extensile stress as observed in certain bacterial suspensions [1]. v_1 is the flow coupling coefficient and $q_{\alpha\beta} = P_\alpha P_\beta - \frac{1}{d}\delta_{\alpha\beta}$. If the coefficient $\xi = 0$ turns off the hydrodynamic coupling is purely passive, which represents the *Model A* with fluid or, as we called it, *Passive Model A*.

The pressure term on the right-hand side of eq. (5) can be eliminated by taking the *curl* ($\nabla\times$) on both sides of eq. (5), we find the equation for the vorticity of fluid $\omega = \nabla\times\mathbf{v}$,

$$\frac{\partial\omega}{\partial t} + (\mathbf{v}\cdot\nabla)\omega = \eta\nabla^2\omega + \nabla\times(\nabla\cdot\sigma^{total}_{\alpha\beta}), \tag{7}$$

by integrating eq. (7), we get ω and then we solve Poisson's equation,

$$\nabla^2\psi = -\omega, \tag{8}$$

where a scalar field ψ is defined such that

$$\mathbf{v} = (\partial_y\psi, -\partial_x\psi). \tag{9}$$

Then the updated flow field $\mathbf{v}(r,t)$ enters eq. (4). We study the ordering kinetics of active polar fluid when quenched from the random disordered state to ordered state. Later everywhere the time and length scales are rescaled by $(a\Gamma_0)^{-1}$ and $\sqrt{\frac{\lambda}{a\Gamma_0}}$, respectively, to make the equations and parameters dimensionless.

We numerically integrate eqs. (4), (7) and (8) using Euler's scheme with small steps $\Delta x = 1.0$ and $\Delta t = 0.1$. In our numerical implementation, the first- and second-order derivatives for an arbitrary function $f(r,t)$ are discretized as

$$\frac{\partial f}{\partial t} = \frac{f(t+\Delta t) - f(t)}{\Delta t}, \tag{10}$$

$$\frac{\partial f}{\partial x} = \frac{f(x+\Delta x) - f(x-\Delta x)}{2\Delta x}, \tag{11}$$

$$\frac{\partial^2 f}{\partial x^2} = \frac{f(x+\Delta x) - 2f(x) + f(x-\Delta x)}{\Delta x^2}. \tag{12}$$

We fix the values of coefficients a, b, λ, η, Γ_0 and v_1 to 1 and tune the activity ξ. The activity ξ is tuned from $[-4, 8]$ to see the effect of both contractile and extensile stresses generated due to fluid present. The system is started from the random homogeneous state of orientation of polarisation and random initial scalar field in the small range $\psi \in [1.0\text{–}1.1]$ and then initial fluid velocity is generated by using eq. (9). After that we calculate the vorticity ω by taking the *curl* ($\nabla\times$) of velocity $\mathbf{v}$. Finally using eqs. (4) and (7) we updated the local polarisation $\mathbf{P}(\mathbf{r},t)$ and vorticity ω, respectively. The further scalar field ψ and velocity $\mathbf{v}$ is updated using Poisson's equation (8) and eq. (9), respectively. This whole process of updates of local polarisation $\mathbf{P}$ and local fluid velocity $\mathbf{v}$ is counted as one simulation step. We let the system evolve for total time steps of $t = 8\times10^4$ (the total real time $t = 8\times10^3$) and system size $L\times L = 512\times512$ and 1024×1024 with periodic boundary conditions in both the directions. The data is averaged over the 25 independent realisations for good statistics. We checked the numerical stability of the system for the present set of parameters.

Results. – We first let the system evolve to the ordered state after a quench from the disordered initial state. After the quench, the point-like defects or disclinations are observed. These defects are a spatially inhomogeneous configuration of the director field or orientational order field in our system. The strength of a disclination depends on the rotation of orientation field around the defect core in one loop. For a two-dimensional system, the rotation of director field can be expressed in terms of a single scalar field, θ, representing the angle formed by the director $n = (\cos\theta, \sin\theta)$ with the horizontal axis of the Cartesian frame. This gives

$$\frac{1}{2\pi}\oint \mathrm{d}\theta = k, \tag{13}$$

where the integral is calculated along an arbitrary contour and k is the winding number. If the contour encloses a defect then the winding number k of vortex/antivortex disclination is $k = +1$ and -1, respectively. For other

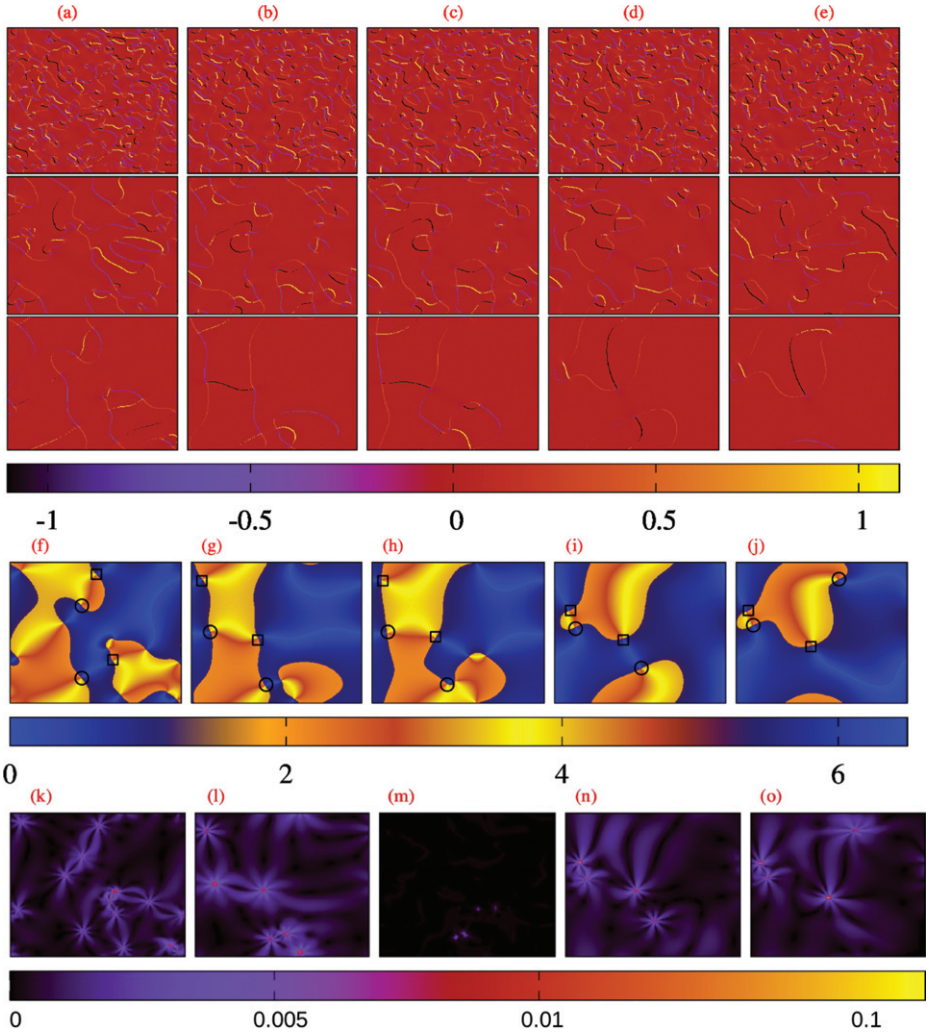

Fig. 1: Panels (a)–(e) are plot of the left-hand size of eq. (13) for different activities $-3, -1, 0, 1$ and 3, respectively. Upper to bottom panels are for different times 80, 800 and 8000. Panels (f)–(j) and (k–o) are corresponding angle $\theta(\mathbf{r}, t)$ and magnitude of fluid velocity $|\mathbf{v}(\mathbf{r}, t)|$, respectively, for the same set of activities as in (a)–(e) and at late time 8000. In (f)–(j) the circles and squares represent the location of some of the vortices and antivortices with winding number $k = +1$ and -1, respectively.

places it should be almost zero. We calculate the value of k for the set of values of activities and variation of k on the two-dimensional plane is shown in fig. 1(a)–(e) for $\xi = -3, -1, 0, 1$ and 3, respectively, and for different times $t = 80$, 800 and 8000, starting from the upper panel to the lower panel. We observe that as the system evolves, the number of defects decreases and the larger value of ξ, the more homogeneous configuration of the orientation field $\mathbf{P}(\mathbf{r}, t)$ is observed. The number of defects decreases by increasing the activity ξ. This we confirm by the angle plot $\theta(\mathbf{r}, t) = \tan^{-1}[\frac{P_2(\mathbf{r},t)}{P_1(\mathbf{r},t)}]$, shown in fig. 1(f)–(j), for the same set of ξ as in fig. 1(a–e) at late time, $t = 8000$. The meeting points of dark and bright colors are the location of defects. The circles and squares in fig. 1(f)–(j) show the locations of some of the vortices and antivortices with winding number $k = +1$ and -1, respectively. Further in fig. 1(k)–(o) we plot the magnitude of fluid velocity $v(\mathbf{r}, t) = |\mathbf{v}(\mathbf{r}, t)|$ for the same set of activities. The structure of fluid is very different for

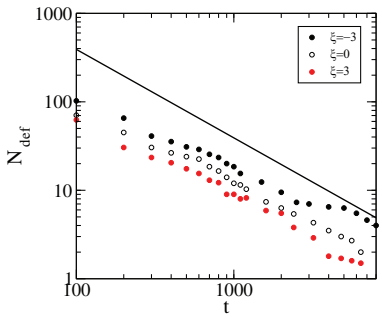

Fig. 2: Number of defects *vs.* time is plotted for three different activities $-3, 0, 3$. The black solid line of slope -1 is drawn.

active and passive cases. Very clearly fluid velocity develops eight-fold symmetric long ranged pattern around the defect cores for active fluid, fig. 1(k), (l), (n) and (o). Such pattern is absent and magnitude of fluid velocity is zero for *passive Model A*, fig. 1(m).

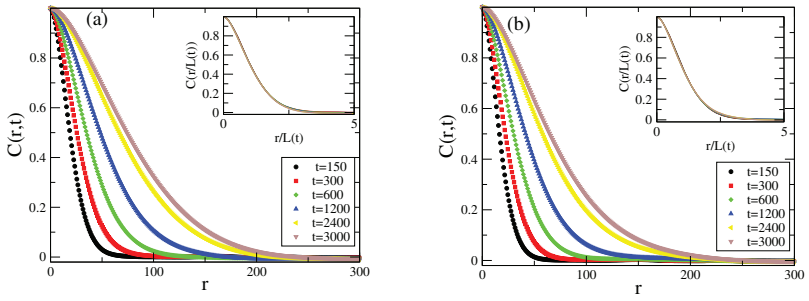

Fig. 3: Two-point correlation function $C(r,t)$ *vs.* distance r at different times for two different $\xi = 3$ and -3 for system size $L = 1024$ in (a) and (b), respectively. The inset figures show the scaled two-point correlation $C(r/L(t))$ *vs.* scaled distance $r/L(t)$.

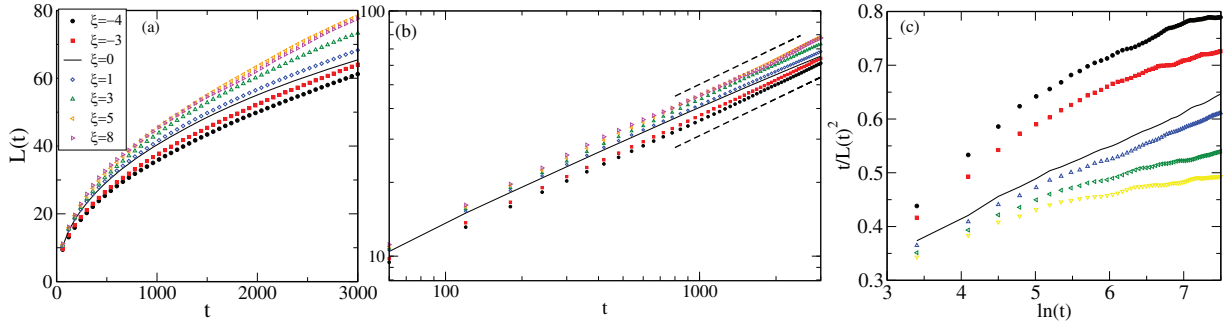

Fig. 4: Panel (a) shows the plot of characteristic lengths $L(t)$ *vs.* time t on linear scale for positive $\xi = 0$, 1, 3, 4 and 5 and for negative $\xi = -3$ and -4. Panel (b) shows the same plot on log-log scale. The two dahsed lines are lines of slope 1/2. (c) The plot of $\frac{t}{(L(t)^2)}$ *vs.* $\ln(t)$ for the ξ's as in (a) and (b).

Next, we quantify the number of defects, N_{def} with time for three different cases, $\xi = -3, 0$ and 3. The N_{def} is calculated by taking the average number of vortices and antivortices or (counting the number of points where the winding number $k = \pm 1$ and then average is performed over 10 independent realisations). From fig. 2, we see that N_{def} decreases with time as power law $\propto t^{-1}$. The higher the activity ξ, the lower the number of defects observed. A solid line of slope -1 is drawn to show the power law decay of N_{def} with time. We further explore the ordering kinetics of the active polar gel for the different activities in the following sections.

Dynamic two-point correlation function. – The nature and evolution of the structure in the orientation field is characterised by calculating the correlations in the orientation order parameter field $\mathbf{P}(\mathbf{r},t)$, defined as $C(r,t) = \langle \delta\mathbf{P}(\mathbf{r}_0 + \mathbf{r}, t) \cdot \delta\mathbf{P}(\mathbf{r}_0, t)\rangle$, where $\delta\mathbf{P}$ is the fluctuation from mean and $\langle \ldots \rangle$ denotes averaging over directions, reference positions r_0 and 25 independent realisations. As the system coarsens with time, correlation function increases as shown in fig. 3 for two different ξ's, 3 and -3, panel (a) and (b), respectively. Further, we define the characteristic length $L(t)$ as the value of r at which the correlation function $C(r,t)$ decreases to 0.1 of its value at $r = 0$. In the insets of fig. 3(a)–(b), we plot the scaled two-point correlations $C(r/L(t))$ *vs.* scaled distance $r/L(t)$. We find that all the curves for different times collapse to a single curve for both contractile $\xi = -3$ and extensile $\xi = +3$ systems. Hence for both the cases the system shows the good dynamic scaling.

Growth law. – We characterise the domain growth by examining the growth law, *i.e.*, the scaling of characteristic length $L(t)$ *vs.* time t for different values and both signs of ξ. In fig. 4(a) we show the variation of characteristic length $L(t)$'s for different ξ *vs.* time t on linear scale. The solid curve in fig. 4(a) is for the *Passive Model A*, whereas the curves on top of it are for extensile case, $\xi > 0$ and below are for the contractile case, $\xi < 0$. Very clearly the characteristic length $L(t)$ decreases on decreasing ξ. In fig. 4(b) we show the same plot on the logarithmic scale. The top and bottom dashed lines have slope 1/2. Clearly for higher magnitude of ξ the curves become closer to $L(t) \sim t^{1/2}$. Hence the hydrodynamic effect in active polar fluid does not affect the asymptotic growth law as found for the nonconserved *Model A* [23]. It only includes a correction factor. Next we give the recipe to estimate the correction factor.

In fig. 4(c) we plot the $t/L^2(t)$ *vs.* $\ln(t)$ for different ξ values, to compare the results with the domain growth of nonconserved two-component vector order parameter field in two dimensions, where $L(t) \sim (t/\ln(L(t))^{1/2}$ [50]. Hence $t/L^2(t)$ should vary linearly with $\ln(t)$. Which is the

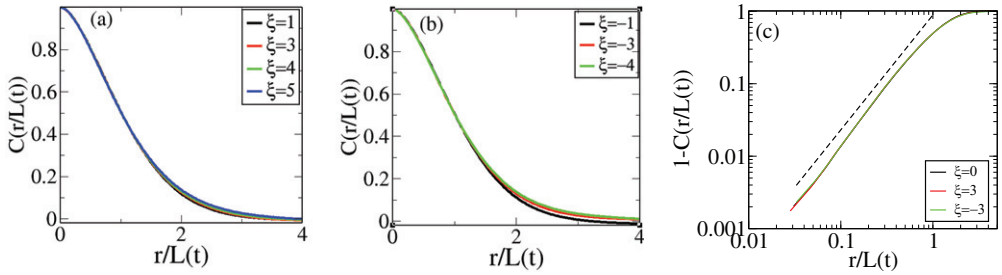

Fig. 5: Static scaled two-point correlation $C(r/L(t))$ *vs.* scaled distance $r/L(t)$ for ξ= 1 , 2, 3 and 5 in (a) and -1, -2 and -3 in (b) for system size $L = 1024$ at fixed $t = 1500$. (c) Plot of $(1 - C(r/L(t))$ *vs.* $r/L(t)$ on log-log scale for different ξ. The dashed line has slope 1.6.

case for passive limit $\xi = 0$ (linear variation of black solid curve) in fig. 4(c). We assume the deviation from the linear dependence or from the *Passive Model A* as a prefactor. The approximated form of characteristic length for finite ξ is $L(\xi, t) = L_0(\xi, t)\big(t/\ln(t)\big)^{1/2}$, where the correction factor $L_0(\xi, t)$ is obtained by the following procedure.

If the growth of domain remains the same as for the *Passive Model A*, then the plot of $t/L^2(t)$ will be linear in $\ln(t)$. We find that for all ξ values for the early times $t/L^2(t)$ plot varies linearly with $\ln(t)$. It remains linear for late time for passive case $\xi = 0$ and smaller activities $|(\xi)| < 3$. Using the expression for the $L(t)$ we can rewrite $t/L^2(t) = \frac{\ln(t)}{L_0^2(t,\xi)}$. For larger times and larger $|\xi| > 3$, the $t/L^2(t)$ plot saturates and becomes independent of time t. Hence the correction $L_0^2(t, \xi)$ should vary as $\sim (\ln(t))$. And the characteristic length simply goes as $L(t) \sim t^{1/2}$, with a constant coefficient decreases with increasing activity. For larger ξ data curve starts to converge. Hence the asymptotic growth becomes pure algebraic, the same as for the nonconserved order parameter with discrete symmetry [23]. The larger active coupling of fluid for high activity case breaks the rotational symmetry present in continuous vector order parameter and leads the system to behave like discrete spins of Ising type [51].

Static two-point correlation function. – We further study the domain morphology for different activities. We calculated the equal-time correlations in orientation order parameter. The equal-time correlation function is defined as before. In fig. 5 we show the plot of equal time scaled two-point correlation function $C(r/L(t))$ *vs.* scaled distance $r/L(t)$ for different activities and fixed time $t = 1500$. The characteristics length $L(t)$ is defined in the same manner. We find that the curves show the deviation from the data collapse when plotted as a function of scaled distance $r/L(t)$ as shown in fig. 3(a),(b) for the extensile and contractile case, respectively. We further characterise the morphology of domains by approximating small distance limit of the scaled two-point correlation function $C(r/L(t)) \simeq (1 - (r/L(t))^{\alpha})$, where α is defined as the cusp exponent [20]. In fig. 5(c) we calculate the cusp exponent α, by plotting $1 - C(r/L(t))$ *vs.* $r/L(t)$ on log-log scale for three different cases: passive $\xi = 0$ and $\xi = 3$ and -3. Although the system does not show the static scaling, for all activities the domain morphology remains the same and is charactrised by the cusp exponent $\alpha \sim 1.6$ and it shows the deviation from the Porod law [52].

Summary. – Now we summarise the work. We study the ordering kinetics of active polar gel. The active gel is defined with 2 collection of orientable objects supplied with active stresses and momentum damping coming from the viscosity of the bulk fluid medium. The activity is controlled by an active stress, which cannot be derived from a free energy. The system can be contractile or extensile depending upon the sign of coupling with the orientation field. We study the growth kinetics of the orientation field, when quenched from the disordered to the ordered state. We find that for the extensile coupling the growth is enhanced and for contractile case it is suppressed with respect to passive system but the asymptotic growth law remains the same as for the nonconserved field. The activity leads to a correction to the growth law of nonconserved vector order parameter. And the asymptotic growth approaches pure algebraic growth for large magnitude of activity. Hence the system behaves equivalently to the scalar nonconserved order parameter field [23]. We have also studied the effect of activity on the dynamic and static scaling of orientation two-point correlation function. The system shows good dynamic and no static scaling for different activities. Domains morphology remains unaffected due to activity and shows a deviation from Porod's law [52]. Our results can be tested on the growth kinetics of wet polar active systems and give a new direction to understand the effect of fluid on the kinetics of orientable objects in fluids.

* * *

SD acknowledges the support and the resources provided by PARAM Shivay Facility under the National Supercomputing Mission, Government of India at the Indian Institute of Technology, Varanasi. SM thanks DST-SERB

India, MTR/2021/000438, andCRG/2021/006945 for financial support.

Data availability statement: The data that support the findings of this study are available upon reasonable request from the authors.

REFERENCES

[1] Marchetti M. C., Joanny J. F., Ramaswamy S., Liverpool T. B., Prost J., Rao Madan and Aditi Simha R., *Rev. Mod. Phys.*, **85** (2013) 1143.
[2] Ramaswamy S., *Annu. Rev. Condens. Matter Phys.*, **1** (2010) 323345.
[3] Rappel W., Nicol A., Sarkissian A., Levine H. and Loomi W. F., *Phys. Rev. Lett.*, **83** (1998) 6.
[4] Berg H. C., *E. coli in Motion* (Springer Science & Business) 2004.
[5] Couzin Iain D., Krause J., Franks Nigel R. and Levin Simon A., *Nature*, **433** (2005) 513516.
[6] Ballerini M., Cabibbo N., Candelier R., Cavagna A., Cisbani E., Giardina I., Lecomte V., Orlandi A., Parisi G., Procaccini A., Viale M. and Zdravkovic V., *Proc. Natl. Acad. Sci. U.S.A.*, **105** (2008) 1232.
[7] Vicsek T., *Phys. Rev. Lett.*, **75** (1995) 1226.
[8] Paxton W. F., Kistler K. C., Olmeda C. C., Sen A., Angelo S. K. St., Cao Y., Mallouk T. E., Lammert P. E. and Crespi V. H., *J. Am. Chem. Soc.*, **126** (2004) 13424.
[9] Bechinger C., Di Leonardo R., Lowen H., Reichhardt C., Volpe G. and Volpe G., *Rev. Mod. Phys.*, **88** (2016).
[10] Wolgemuth C. W., *Biophys. J.*, **95** (2008) 1564.
[11] Toner J. and Tu Y., *Phys. Rev. E*, **58** (1998) 4828.
[12] Ramaswamy S., Simha R. A. and Toner J., *Europhys. Lett.*, **62** (2003) 196.
[13] Toner J., Tu Y. and Ramaswamy S., *Ann. Phys.*, **318** (2005) 170.
[14] Chate H., Ginelli F., Grégoire G. and Raynaud F., *Phys. Rev. E*, **77** (2008) 046113.
[15] Mishra S., Tunstrom K., Couzin I. D. and Huepe C., *Phys. Rev. E*, **86** (2012) 011901.
[16] Das R., Mishra S. and Puri S., *EPL*, **121** (2018) 37002.
[17] Mishra S., Puri S. and Ramaswamy S., *Philos. Trans. R. Soc. A*, **372** (2014) 20130364.
[18] Pattanayak S., Mishra S. and Puri S., *Phys. Rev. E*, **104** (2021) 014606.
[19] Wittkowski R., Tiribocchi A., Stenhammar J., Allen R. J., Marenduzzo D. and Cates M. E., *Nat. Commun.*, **5** (2014) 5351.
[20] Bray A. J., *Adv. Phys.*, **43** (1994) 357.
[21] Puri S., *Kinetics of Phase Transitions* (CRC Press) 2008.
[22] Lifshitz I. M. and Slyozov V. V., *J. Phys. Chem. Solids*, **19** (1961) 35.
[23] Hohenberg P. C. and Halperin B. I., *Rev. Mod. Phys.*, **49** (1977) 435.
[24] Allen S. M. and Cahn J. W., *Acta Metall.*, **27** (1979) 1085.
[25] Wagner C., *Z. Electrochem.*, **65** (1961) 581.
[26] Blundell R. E. and Bray A. J., *Phys. Rev. E*, **49** (1994) 6.
[27] Mondello M. and Goldenfeld N., *Phys. Rev. A*, **42** (1990) 10.
[28] Tiribocchi A., Wittkowski R., Marenduzzo D. and Cates M. E., *Phys. Rev. Lett.*, **115** (2015) 188302.
[29] Navarro R. M. and Fielding S. M., *Soft Matter*, **11** (2015) 7525.
[30] Alarcon F. and Pagonabarraga I., *J. Mol. Liq.*, **185** (2013) 56.
[31] Llopis I. and Pagonabarraga I., *Europhys. Lett.*, **75** (2006) 999.
[32] Julicher F., Kruse K., Prost J. and Joanny J.-F., *Phys. Rep.*, **449** (2007) 3.
[33] Simha R. A. and Ramaswamy S., *Phys. Rev. Lett.*, **89** (2002) 5.
[34] Elgeti J., Cates M. E. and Marenduzzo D., *Soft Matter*, **7** (2011) 3177.
[35] Thampi S. P., Golestanian R. and Yeomans J. M., *EPL*, **105** (2014) 18001.
[36] Giomi L., *Phys. Rev. X*, **5** (2015) 031003.
[37] Pattanayak S., Mishra S. and Puri S., *Soft Mater.*, **19** (2021) 286.
[38] Kumar S. and Mishra S., *Phys. Rev. E*, **106** (2022) 044603.
[39] Voituriez R., Joanny J. F. and Prost J., *Europhys. Lett.*, **70** (2005) 404.
[40] Marenduzzo D., Orlandini E., Cates M. E. and Yeomans J. M., *Phys. Rev. E*, **76** (2007) 031921.
[41] Kruse K., Joanny J. F., Jülicher F., Prost J. and Sekimoto K., *Phys. Rev. Lett.*, **92** (2004) 078101.
[42] Saha S., Das A., Patra C., Anilkumar A. A., Sil. P., Mayor S. and Rao M., *Proc. Natl. Acad. Sci. U.S.A.*, **119** (2022) 30.
[43] Prost J., Julicher F. and Joanny J.-F., *Nat. Phys.*, **11** (2015) 111.
[44] Fielding S. M., Marenduzzo D., 2 and Cates M. E., *Phys. Rev. E*, **83** (2011) 041910.
[45] Chaikin P. M. and Lubenskey T. C., *Principles of Condensed Matter Physics* (Cambridge University Press) 1995.
[46] Kim B. J., Minnhagen P. and Olsson P., *Phys. Rev. B*, **59** (1998) 17.
[47] Orihara H., Fukase A., Izumi S. and Ishibashi Y., *Ferroelectrics*, **147** (1993) 411.
[48] Kruse K., Joanny J. F., Julicher F., Prost J. and Sekimoto K., *Eur. Phys. J. E*, **16** (2005) 5.
[49] Simha R. A. and Ramaswamy S., *Physica A*, **306** (2002) 262.
[50] Bray A. J., *Phys. Rev. B*, **41** (1990) 10.
[51] Yang C. N., *Phys. Rev.*, **85** (1952) 808.
[52] Porod G., *Kolloid Z.*, **83** (1951) 124.